

Strike Slip Motion and the Triggering of Subduction Initiation

Yida Li, Michael Gurnis

Seismological Laboratory, California Institute of Technology, Pasadena, CA 91125, USA

Correspondence*: Yida Li yidali@caltech.edu

2 ABSTRACT

Plate tectonic reconstructions of three of the best-defined Cenozoic subduction initiation (SI) 3 events in the western Pacific, Izu-Bonin-Mariana, Vanuatu, and Puysegur subduction zones, show substantial components of strike-slip motion before and during the SI. Using computational 5 models, we show that strike-slip motion has a large influence on the effective strength of incipient margins and the ease of SI. The parameter space associated with visco-elasto-plastic rheologies, plate weakening, and plate forces and kinematics is explored and we show that subduction initiates more easily with a higher force, a faster weakening, or greater strike-slip motion. With 9 the analytical solution, we demonstrate that the effect of strike-slip motion can be equivalently 10 represented by a modified weakening rate. Along transpressive margins, we show that a block 11 of oceanic crust can become trapped between a new thrust fault and the antecedent strike-slip 12 fault and is consistent with structural reconstructions and gravity models of the Puysegur margin. 13 Together, models and observations suggest that SI can be triggered when margins become 14 15 progressively weakened to the point that the resisting forces become smaller than the driving forces, and as the negative buoyancy builds up, the intraplate stress eventually turns from 16 17 compressional into extensional. The analytical formulation of the initiation time, t_{SI} , marking the moment when intraplate stress flips sign, is validated with a computational models. The analytical 18 19 solution shows that t_{SI} is dominated by convergence velocity, while the plate age, strike-slip velocity, and weakening rate all have a smaller but still important effect on the time scale of SI. 20

21 Keywords: geodynamics, subduction, subduction initiation, faults, plate kinematics

1 INTRODUCTION

Consensus on a unified description of subduction initiation has been slow to develop as initiation is a transient process whose record is generally obscured by subsequent subduction zone processes, notably 23 24 burial, overprinting, uplift, and compression and over-thrusting. Nevertheless, there is a substantial 25 geological record with nearly all ocean-ocean subduction zones having initiated since the end of the 26 Mesozoic and about half of all ocean-continent ones having re-initiated since the mid-Mesozoic (Hu and 27 Gurnis, 2020). Subduction initiation, moreover, occurs nearby existing subduction zones (Crameri et al., 2020), is a fundamental component of plate tectonics, and is putatively associated with key changes in the 28 force balance of tectonic plates. For example, the Pacific Plate changed its direction of motion from NNW 29 to NW at around 50 Ma (Whittaker et al., 2007; Torsvik et al., 2017), synchronously with the initiation of

40

41

42

43

44 45

46

47

48

49

50 51

52

53

54

55

56

57

58

59

60

61 62

63

64

66

67

two major subduction zones in the western Pacific, the Izu-Bonin-Mariana (IBM) (Ishizuka et al., 2018; Reagan et al., 2019) and Tonga-Kermadec (Sutherland et al., 2020). However, why new subduction zones form remains poorly understood, as subduction initiation appears to be mechanically unfavorable with initial slab pull being insufficient to overcome resistance from the friction between plates and bending of the slab (McKenzie, 1977; Toth and Gurnis, 1998; Li and Gurnis, 2022). An external force, or low initial strength between plates, is required to start subduction, with scenarios for initiation described as either spontaneous (Stern and Bloomer, 1992; Nikolaeva et al., 2010) (with no external force but low strength) or induced (Gurnis et al., 2004; Toth and Gurnis, 1998) (with an external force).

With theoretical and computational approaches, the thermal age of plates, compositional variations, trench-normal convergence and in-plane stress (Gurnis et al., 2004; Nikolaeva et al., 2010; Leng and Gurnis, 2011) and fault strength, fault weakening and plate bending (McKenzie, 1977; Toth and Gurnis, 1998; Thielmann and Kaus, 2012; Qing et al., 2021) having been identified as key mechanical factors which respectively drive and limit subduction initiation. Independent of spontaneous and induced scenarios, driving forces must overcome frictional resistance between plates and bending of the high, effective viscosity plate. If the plate boundary does not weaken sufficiently fast, the oceanic plate will not slide into the mantle to allow the negative thermal buoyancy to grow quickly enough. Constitutive models with strength that weakens with deformation, due to grain size reduction, grain damage, or volatile ingestion, have been identified (Thielmann and Kaus, 2012; Bercovici and Ricard, 2014; Hirth and Kohlstedt, 1996) and can lead to rapid instability (Leng and Gurnis, 2015; Zhou et al., 2018). Models exhibiting spontaneous initiation start in a critical state that verges on instability (Leng and Gurnis, 2015; Zhou et al., 2018), an unsatisfactory condition to address causes for the onset of initiation. If a plate boundary is in a state close to instability, the question arises as to why the boundary initiated at that point in time and not earlier.

Strike-slip motion might be one reason plate boundaries are brought closer to a state favorable for subduction initiation. Plate tectonic reconstructions of the IBM, Vanuatu and Puysegur subduction zones, three of the best constrained subduction initiation events in the western Pacific during the Cenozoic, each show a substantial component of strike-slip motion before and during initiation (Fig. 1). The Puysegur subduction zone extending south from the South Island of New Zealand has a well-documented component of strike-slip motion during subduction initiation which continues to the present (Lamarche and Lebrun, 2000; Sutherland et al., 2006). The initiation of IBM, among the best studied and often used as a point of comparison with other subduction zones, ophiolite-origin models, and mechanical models (Arculus et al., 2019). Although less discussed, IBM experienced a strong component of strike slip motion during the well-documented period of initiation (Gurnis, 2023). The Vanuatu subduction initiation also saw a strong component of strike-slip motion during the interval 15 to 12 Ma when the new subduction zone was forming through a polarity reversal with velocities of about 5 to 6 cm/yr (Fig. 1B, D). In addition to the the main Vanuatu subduction zone, a new segment of the plate boundary is initiating at its southern boundary, referred to as the Matthew and Hunter subduction zone, with a small 2 cm/yr convergence and a subtantially larger strike-slip motion along the Hunter Ridge since 2 Ma (Patriat et al., 2019). All of these subduction initiation events must have been shaped by strike-slip motion, but do large components of strike-slip motion influence the mechanics of initiation?

2 MODEL FORMULATION

70 We solve for the Stokes equations using traditional formulations used in geodynamics (Moresi et al.,

71 2000; Ismail-Zadeh and Tackley, 2010) and show that a component of strike-slip motion can substantially

2 reduce the strength of a nascent plate boundary while providing a triggering mechanism to nucleate a

new subduction zone. The idea that strike-slip motion produces a more favorable condition for the far-74 field compression to induce subduction is examined by Zhong and Li (2023) with 3D models. Here, we address this problem with a sliced 3D geometry extended from the trench-perpendicular cross-section (x-z 75 76 dimension), with an additional trench-parallel dimension (y-dimension) that accounts for the strike-slip 77 motion (Fig S1). In the trench-perpendicular (x-z) dimension, we apply either a convergent velocity or a convergent force on the right side of the subducting plate to induce subduction initiation. In the trench-78 79 parallel dimension, a strike-slip velocity is applied on the right wall of the subducting plate to drive the 80 strike-slip velocity. For the two boundaries normal to the strike direction, we apply a periodic boundary condition, which allows the material to flow through the two boundaries freely. As the width of the trench 81 82 parallel dimension is small (≈ 6 km) with only two layers of elements and periodic boundary conditions enforcing the strike-slip velocity, the models virtually solve for a plane strain problem with no variation 83 along strike. 84

A younger overriding plate is to the left of an old oceanic plate with either a compressional force or a convergent velocity added on the right edge of the older plate. A pre-existing weak zone with yielding stress being reduced by half is located at the plate boundary. As plate convergence and strike-slip motion accumulates, the strain will eventually localize at the plate boundary.

The deformation of a visco-elasto-plastic material is computed with the finite element code *Underworld* (Mansour et al., 2019). The constitutive relationship between strain rate, $\dot{\varepsilon}$, and deviatoric stress, τ , is defined through a visco-elastic Maxwell body (Moresi et al., 2003),

$$\dot{\varepsilon} = \frac{\dot{\tau}}{2\mu} + \frac{\tau}{2\eta} \tag{1}$$

92 Viscosity follows the non-Newtonian Arrhenius law

$$\eta = \eta_0 (\frac{\dot{\varepsilon}_{II}}{\dot{\varepsilon}_0})^{\frac{1}{n} - 1} e^{\frac{E}{nR} (\frac{1}{T} - \frac{1}{T_0})}$$
 (2)

where μ is the shear modulus, η the viscosity, T the temperature, and $\dot{\varepsilon}_{II}$ the second invariant of strain rate tensor. E, n and R are activation energy, non-linear exponent, and ideal gas constant. $\dot{\varepsilon}_0$, η_0 and T_0 are reference strain rate, reference viscosity and reference temperature.

Plasticity, describing the strength of the rock, is an essential component of subduction initiation. We assume a yielding envelope given by the Drucker-Prager failure criteria bounded by a maximum stress

$$\tau = \min(C\cos\phi + P\sin\phi, \tau_{max}) \tag{3}$$

98 where τ is the yielding envelop, C and ϕ are cohesion and friction angle and τ_{max} the maximum stress 99 the rock can sustain. With the accumulation of plastic strain, the yielding envelope is reduced through 100 rock damage or grain size reduction. The weakening is approximated as a two-stage process: The yielding 101 envelope first reduces linearly with increasing plastic strain until saturation at which point the plastic 102 parameters C and ϕ remain constant.

$$C = C_0 + (C_f - C_0) \min(1, \frac{\varepsilon_P}{\varepsilon_{P0}})$$
(4)

 $\phi = \phi_0 + (\phi_f - \phi_0) \min(1, \frac{\varepsilon_P}{\varepsilon_{P0}})$ (5)

- The reference plastic strain, ε_{P0} , controls the weakening rate with rocks weakening faster with smaller ε_{P0} and vice versa. With a lack of consensus on the underlying mechanisms responsible for weakening
- 106 (Thielmann and Kaus, 2012; Bercovici and Ricard, 2014; Hirth and Kohlstedt, 1996), ε_{P0} is varied as an
- 107 unknown along with other key parameters including the external compression, F_{xx} , and strike-slip velocity,
- 108 V_{SS} . Details of model parameters are in Supplementary Table 1.
- In addition to the numerical models, we formulate an analytical solution modified from Li and Gurnis
- 110 (2022) considering the extra influence of the strike-slip motions. The formulation of the analytical solution
- is based on the horizontal force balance of the subducting plate between the forces that drive the plate
- 112 motion and forces that resists plate motion. The strike-slip motion affects the force balance equation
- through accelerating the weakening process, thereby reducing the frictional resistance at the plate boundary.
- 114 By varying modeling parameters of interest, like the strike-slip velocity and weakening rate, we measure
- quantities like the plate force, F_{xx} , initiation time, t_{SI} , and total work, W_{SI} , from numerical models, that
- are compared with the analytical predictions.

3 RESULTS

117

3.1 Kinematic boundary condition

- We use a kinematic boundary condition with a constant convergent velocity on the right end of the 118 119 subducting plate to initiate subduction (Fig S1A, Fig 2A). The different conditions controlling the evolution of subduction are evaluated by tracking the vertically-integrated horizontal compressional stress in the 120 plate, i.e. $F_{xx} = \int_0^{d_{lith}} -\sigma_{xx} dz$, where d_{lith} is the thickness of lithosphere. Prior to initiation, plate motion 121 is resisted by a large coupling stress at the plate boundary. Later, F_{xx} drops with plate convergence, ℓ , 122 through plastic weakening and decoupling of the two plates and accumulation of negative buoyancy (Li 123 and Gurnis, 2022). Eventually, F_{xx} becomes negative (extensional), indicating that subduction has become 124 self-sustaining and driven by the negative buoyancy of the slab instead of external forces (Fig. 2B-C), and 125 we define the time when F_{xx} drops to 0 as the initiation time t_{SI} . Following Li and Gurnis (2022), we 126 define the total work, W_{SI} , done by the boundary velocity to induce a subduction initiation until t_{SI} (i.e. 127 $W_{SI} = \int_0^{t_{SI}} F_{xx} V_x dt$), characterizing the total resistance that the driving force overcomes. The tracking of 128 plate force, initiation time, and total work quantitatively reflect the difficulty to induce subduction initiation. A larger F_{xx} , t_{SI} and W_{SI} indicate the subduction initiation encounters greater resistance. We develop an 130 analytical solution of the strike-slip subduction initiation model, validate it with the numerical results, and 131 expand the parametric space via the analytical solution.
- In 2D cross-sectional models (with no strike-slip motion), F_{xx} can be formulated analytically via a force 133 balance analysis on the subducting plate, such that F_{xx} , together with slab pull as the driving force, is 134 balanced by the resistance from plate bending, inter-plate friction, isostatic gradients at the boundary, and 135 shear from mantle flow (Li and Gurnis, 2022). The addition of the third dimension (strike-slip) mainly 136 changes the system by enhancing the weakening process. To analytically address the role of strike slip 137 motion, we modify the formulation of inter-plate friction by enhancing the weakening as a result of the 138 strike-slip velocity (see Supplementary material section S1). The contribution of strike-slip motion is 139 analytically shown to be equivalent to reducing the effective weakening rate $\varepsilon_{P0_eff} = \varepsilon_{P0} \frac{v_x}{\sqrt{V_x^2 + V_{SS}^2}}$ 140 and thereby reduce the inter-plate friction. This friction is balanced by the driving force, F_{xx} , and the 141 analytical model (dashed line in Fig 2B-C) predicts a decrease of F_{xx} with increasing V_{SS} , in agreement 142 with the numerical models (solid line in Fig 2B-C). Increasing strike-slip velocity and weakening rate 143 consistently lowers F_{xx} , as both reduce the resistance inhibiting subduction initiation. A grid search of 144

- 145 V_{SS} and ε_{P0} shows how these parameters influence W_{SI} (Fig. 2 D). In the limit of a small V_{SS} and a large
- 146 ε_{P0} , convergence is insufficient to nucleate a weak zone and initiate a subduction (open circles, Fig. 2 D).
- Outside of that domain, subduction initiates and the resistance has a consistent trend: Increased V_{SS} and
- 148 decreased ε_{P0} tend to lower W_{SI} .
- Finally, we evaluate t_{SI} from the analytical model varying V_x , V_{SS} , ε_{P0} and subducting plate age
- 150 (Fig 3). As discussed in Li and Gurnis (2022), the initiation time is dominantly controlled by the total
- 151 plate convergence, so that convergence rate V_x has a first-order control on the predicted t_{SI} . Subducting
- 152 plate age determines the plate thickness, which controls both the plate bending resistance and the slab
- pull. The plate age affects the force balance in two ways, the slab pull and plate bending because the plate
- 154 thickness changes. As the dependence of slab pull on plate thickness is first order while plate rigidity (with
- plasticity) second order, the change of t_{SI} is dominated by slab pull when plate is young (< 10 Ma), and
- 156 for an old plate (> 20 Ma) the t_{SI} is governed by plate bending. Therefore, below 10Ma we see a decrease
- 157 of t_{SI} as the plate gets older due to increased slab pull that drives plate motion, while above 20 Ma t_{SI}
- 158 increases with plate age due to increased bending resistance. Both V_{SS} and ε_{P0} influence t_{SI} via the term
- 159 of inter-plate friction. Both increase of V_{SS} and decrease of ε_{P0} lead to an acceleration of subduction
- initiation, thereby reducing the t_{SI} . However, compared to V_x , the impact of the plate age, V_{SS} and ε_{P0} is
- 161 minor.

162 3.2 Force Boundary Conditions

- Besides an applied convergent velocity, subduction initiation can be induced through applying a force on the edge of the plate (Fig. S1B). We use a geometry approximating a mid-ocean ridge and a compressional force F_{xx} at the ridge edge of the subducting plate (Fig. S1). The total compression driving the plate motion is composed of the internal ridge push from the thermal contrast and the external force F_{xx} . When F_{xx} is sufficiently large, plate bending and resistance by shearing between plates at the nucleating boundary are overcome with subduction initiation (Leng and Gurnis, 2011; Zhong and Li, 2019); the minimum force
- 169 needed for initiation is determined through systematic variation of parameters.
- All prior models of subduction initiation in the literature have no strike-slip motion, and so we start
- 171 with a case with no strike-slip velocity with $[\varepsilon_{P0}, V_{SS}, f_{xx}]$ =[2, 0 cm/yr, 8.57 × 10¹² N/m], as a
- 172 reference (Fig. S2B) In this case, due to the insufficient compression to induce subduction initiation
- 173 $(F_{xx} = 8.57 \times 10^{12} \text{ N/m})$ under a relatively low weakening rate $(\varepsilon_{P0} = 2, \text{ larger } \varepsilon_{P0} \text{ meaning slower})$
- 174 weakening), the subduction initiation fails to occur and the plate boundary remains stable (Fig. S2B).
- 175 Typical ridge push forces range from 2 to 4×10^{12} N/m (Bott, 1991; Toth and Gurnis, 1998) and so
- 176 the F_{xx} used is not particularly small. Over time, the plate boundary remains stable with no subduction
- being induced. By taking this case as a reference, and then by either adding a V_{ss} of 2 cm/yr (Fig. S2C),
- 178 or decreasing ε_{P0} from 2 to 1 (such that the fault weakens faster), the plate boundary initiates into a
- 179 subduction zone (Fig. S2D). This shows that the presence of strike-slip motion and acceleration of the
- 180 weakening process independently facilitate subduction initiation.
- The key parameters, including strike-slip velocity, external compression, and the weakening rate, are systematically varied while computing the initiation time (Fig. S3). The grid search shows that regardless of the choice of weakening rate and resolution, increased strike-slip velocities lower the minimum required
- 184 compressional force (Fig. S3 thick lines) for subduction to initiate. A lower ε_{P0} (faster weakening) always
- 185 reduces the required external force, therefore facilitating subduction initiation. Unlike the velocity boundary
- 186 model where the strike-slip velocity has a minor influence on plate stress and initiation time, the addition

of strike-slip motion significantly reduces the stress required to initiate a subduction zone (solid curves in Fig S3, S4), indicating the strike-slip motion provide a more favorable condition for subduction initiation.

189 3.3 Fault Evolution

The computations yield a fault system that evolves from a single strike-slip fault into a strain partitioned system composed of a vertical strike-slip fault and a dipping oblique thrust fault with partitioning of strike-slip velocity between the two (Fig. 4). Initially, the plate boundary fault is vertical, and will remain so with only subsequent strike-slip motion; however, subduction requires a dipping thrust fault to decouple the two plates. In those cases where the system evolves into a subduction zone, we have found that the thrust fault emerges through the combined reuse of the strike-slip fault and new fault formation. The upper part of a trapped block is bound by a vertical strike-slip fault and an oblique thrust fault as the upper lithosphere has a high viscosity and brittle failure (faulting) is the dominant mechanism that accommodates the compression. The lower part of the vertical strike-slip fault rotates with compression of the somewhat lower viscosity, ductile lower lithosphere. Through this process, the lower part of the vertical strike-slip fault is transferred and becomes the lower part of the oblique thrust fault. The reuse of a vertical fault weakened by strike-slip motion is a primary reason why strike-slip motion can lower the required force to induce subduction and therefore facilitate subduction initiation.

In the case shown above, we choose a high yield stress (300 MPa) which makes the crust of the overriding plate strong. However, with a continental upper plate with a weaker crustal layer, the resultant morphology is different (Fig. S5). In this case, the rheology yields a typical continental strength envelope (Kohlstedt et al., 1995), with a weak layer present at the base of the continental crust, decoupling the lithosphere from the crust. Unlike the strong plate case where a new dipping fault emerges in the upper part of the subducting plate in response to the far–field compression, in the case of weak continental crust, the overriding plate severely deforms to accommodate the compression. In the overriding plate, the lower lithosphere delaminates at the base of the buoyant continental crust. The compression forces the subducting plate and the lower lithosphere of the upper plate to bend simultaneously, and a vertical strike-slip fault emerges in the upper plate crustal layer to reconcile the strike-slip motion. Consequently, a strain partitioning system emerges, but the wedge trapped between the strike-slip fault and the dipping thrust fault is composed of continental crust.

4 DISCUSSION

With the numerical models that extend a traditional 2D trench perpendicular cross-sectional domain with orthogonal strike-slip motion, such motion influences subduction initiation. This builds on the concept that mature strike-slip faults like the San Andreas Fault (SAF) are weak (as revealed through stress indicators (Zoback et al., 1987) and heat flow (Brune et al., 1969)) and that the damage around faults grows with increasing fault displacement (Faulkner et al., 2011; Savage and Brodsky, 2011). A common conceptual idea is that a strike-slip fault will have local irregularities along the strike such there will be zones of convergence that could be sites for subduction initiation. A well-known example where local transpression leads to downwelling, although not subduction initiation, is the Miocene evolution of the San Andreas Fault (SAF) and Transverse Ranges of southern California in North America. Here, it is thought that the clear convergence across the Big Bend segment of the SAF north of Los Angeles has led to crustal and lithospheric thickening and convective instability (Humphreys and Clayton, 1990). However, we present a scenario that is distinctly different from this one, advancing the hypothesis that even with no irregularities in the orientation of faults along strike, subduction initiation is enhanced by strike-slip motion.

Can the models be applied to specific subduction initiation events? An obvious application is along the boundary between the Pacific and Australian Plates, south of New Zealand, the Puysegur subduction zone (Fig. 1E). Here, a major strike-slip fault immediately to the east of the trench accommodates some of the relative plate motion (Collot et al., 1995; Lamarche and Lebrun, 2000). The age of the Puysegur subduction zone has been estimated in two ways. First is through a reconstruction using a combination of the depth extent of the seismic slab and plate kinematics, which date the onset of subduction to between 15 and 12 Ma (Sutherland et al., 2006). Second, the age has been estimated through detailed seismic imaging of the stratigraphy on the overriding Pacific Plate which shows basin inversion (Shuck et al., 2022). In the northern section of Puysegur, the compression starts at 15 Ma and transitions to mild extension by 8 Ma. During this interval, most of the relative motion between the Australian and Pacific Plates was strike-slip with velocities of about 3 cm/yr (Fig. 1B). The subducting plate at Puysegur Trench formed along the Macquarie Ridge Complex (MRC) system, where sea-floor spreading was active since the Eocene (about 40 Ma) but terminating at about 15 Ma (Lebrun et al., 2003). The subducting plate age ranges from 25 Ma (north) to 5 Ma (south). With the given range of V_x , V_{SS} , and plate age for Puysegur, we predict a range of t_{SI} from the analytical model (Fig 3, blue box). The northern Puysegur trench corresponds to the top right corner of the blue box ($V_x = 1$ cm/yr, plate age = 25 Ma), yielding a model $t_{SI} \approx 12$ Myr which roughly agrees with the observed 8 Myr duration for the basin inversion (16 to 8 Ma). For the southern Puysegur, the analytical model yields a larger t_{SI} (> 30 Myr) given the small V_x (≈ 0.2 cm/yr) and young subducting plate (5 Myr old) at 15 Ma. This prediction may over-estimate t_{SI} as during the subduction initiation the convergent velocity V_x increases substantially from 0.2 cm/yr at 15Ma to ~ 2 cm/yr today due to the change of plate motion direction (Choi et al., 2017), and the large predicted t_{SI} sheds light on why the southern Puysegur remains under compression today – in addition to the hypothesis of southward propagation of subduction initiation proposed in Shuck et al. (2022).

Puysegur has other features reflective of the initiation phase as it evolved from a strike-slip boundary to transpressional since 16 Ma, in particular a sliver of oceanic crust (Hightower et al., 2020) trapped at the Puysegur Trench, bounded by a vertical fault and an oblique thrust fault (Collot et al., 1995; Shuck et al., 2022). East of the Puysegur Trench, the morphology of the Puysegur Fault through the central part of the southern Puysegur Ridge is sharp and consistent with present-day activity (Shuck et al., 2021). The 2009 Mw 7.8 Dusky Sound earthquake below Fiordland, the strike-slip onshore extension of the nascent subduction zone, showed that nearly all of the relative motion, including the strike-slip motion, was accommodated on the thrust interface (Beavan et al., 2010). Consequently, the seismic imaging and 2009 event for Puysegur shows that it has a structure, morphology, and strain partitioning consistent with that shown in Figure 4, that is with substantial strike-slip motion on the thrust interface, and the entrapment of an oceanic sliver between the newly formed thrust interface and the strike-slip fault.

Subduction along IBM initiated at the boundary between the Pacific Plate and the smaller West Philippine Sea Plate along the Kyushu Palau Ridge (Fig. 1C). The new subduction zone is inferred to have formed between 52 and 50 Ma as indicated by ages within the forearc (Reagan et al., 2019) and basement of the West Philippine Sea Plate (Ishizuka et al., 2018). IBM is often viewed as a type locality for studying subduction initiation because of the rock record on the IBM fore—arc and an association with changes in Pacific Plate motion during the Cenozoic (Stern and Bloomer, 1992; Arculus et al., 2019). The IBM subduction zone may be an example of spontaneous subduction initiation (Stern and Bloomer, 1992), with a short, rapid burst of localized extension (Reagan et al., 2019). The overriding Philippine Sea Plate had a relic arc with thick buoyant crust adjacent to the old, cold Pacific plate at the location of apparent subduction initiation and this may have played a role in its initiation (Leng and Gurnis, 2015). Computational models suggest that compression of the incipient plate margin needs to overcome a large resisting force associated

with bending the incipient slab (Gurnis et al., 2004; Li and Gurnis, 2022), but there is debate in the literature on the significance of the compression. On the one hand, Maunder et al. (2020) argued that early compression cannot lead to near–field extension and boninite formation and that a large vertical force is needed for such extension, a force which only can exsit if there is pre-existing subduction. Moreover, a recent interpretation of Baron isotope systematics on IBM forearc recovered samples apparently indicate an initial low–angle phase of thrusting prior to the formation of the distinctive basalt to boninite sequence (Li et al., 2022).

Although not widely discussed, several lines of evidence suggest that there was a strong component of strike-slip motion during IBM inception. Paleomagnetic observations show that since 50 Ma, the Philippine Sea Plate experienced nearly 90° of clockwise rotation (Hall et al., 1995); since the orientation of the Kyushu-Palau Ridge (the relic arc that formed at the new boundary) is currently N-S, it would have been more E-W during subduction initiation. The orientation of convergence between the West Philippine Sea and Pacific Plates depends on the absolute motion of the Pacific Plate, but the Pacific moved by the overriding plate in a mostly strike-slip orientation with velocities of about 5 cm/yr for at least five million years before initiation (Fig. 1 B,C), with V_{SS} and V_x varying substantially along strike due to the curved plate boundary. Independently, detailed bathymetry just to the west of the Kyushu Palau Ridge reveal a strike-slip fault subparallel and normal faults perpendicular to the ridge in which the basement dates to the time of subduction inception, 49 Ma (Gurnis, 2023). This is consistent with transverse motion along the KPR at the time of initiation. Nearly identical forearc volcanic stratigraphy near the Bonin Islands and near Gaum Islands, 500 km apart when plate tectonic motions are accounted for (Leng and Gurnis, 2015), could have been further seperated by strike slip motion.

The strike-slip model of induced subduction initiation can be applied to IBM. With subducting plate age varying between 40 and 60 Myr old at 50 Ma (Hall et al., 2003; Lallemand and Arcay, 2021), the analytical model yields a range of initiation times (Fig 3). At 55 Ma, the predicted t_{SI} range from 5 to 10 Myr with $V_{SS} = 3$ to 6 cm/yr. At 50 Ma, the reconstruction gives a larger range of V_{SS} (0 to 6 cm/yr), and the analytical model predicts a $t_{SI} \approx 3$ to 5 Myr. Using the plate tectonic constraints at 55 Ma and 50 Ma, we estimate the time for the IBM to experience conversion from compression to extension to be around 50 to 45 Ma, a 5 Myr duration slightly larger than the 2 Myr inferred from fore–arc opening determined from $^{40}\mathrm{Ar}/^{39}\mathrm{Ar}$ and U-Pb ages of the boninite-basalt sequence in the IBM fore–arc (52 to 50 Ma) (Reagan et al., 2019).

IBM subduction initiation may be associated with the shift in Pacific Plate motion from more northerly before 50 Ma to more westerly after 50 Ma, as evident from plate reconstructions and the bend in the Hawaiian–Emperor Seamount chain (e.g. Torsvik et al. (2017) and Müller et al. (2019)). Hu et al. (2022) showed that Pacific Plate motion could change by about 10° (from more northerly to northwesterly) with introduction of the IBM slab from 55 to 50 Ma. Most of the required change in absolute Pacific Plate motion must come from elsewhere, and Hu et al. (2022) show that this can be accomplished with termination of intra-oceanic subduction in the north Pacific between 55 and 50 Ma. Other west Pacific subduction zones forming during the Cenozoic, however, may have initially been induced, including the Tonga-Kermadec subduction zone that underwent vertical motions and folding within the future back-arc region prior to and contemporaneously with subduction initiation, indicating a strong compressive force during initiation (Sutherland et al., 2020). Strike–slip motion between Pacific and West Phillipine Sea Plates, along with compression along this boundary due to rearrangement of Pacific Plate driving forces can lead to IBM subduction initiation. The models favor an induced mode of subduction initiation, as the minimum stress (Fig. S3 solid lines) never vanishes independent of the magnitude of V_{SS} .

317 The Vanuatu subduction zone initiated between 12 and 10 Ma, following the collision of the Ontong-Java 318 Plateau with the Vitiaz subduction zone at 16 Ma (Mann and Taira, 2004) and may be an example of induced subduction polarity reversal (Auzende et al., 1988; Yang, 2022). Soon after Vanuatu subduction 319 320 initiation, the Fiji basin opens at ~ 8 Ma, indicating a short initiation time (Auzende et al., 1988; Lallemand 321 and Arcay, 2021). The plate reconstructions show a strong component of strike-slip motion (5-8 cm/yr), Fig 1.B dashed blue curve) between the Australian and Pacific plates along the Vanuatu incipient boundary 322 323 (Fig. 1B,D) The strike-slip mechanical model yields a small value for t_{SI} (≈ 3 Myr, Fig 3), because of the large strike-slip velocity V_{SS} , large convergent velocity V_x and the young plate age (Lallemand and Arcay, 324 325 2021).

5 CONCLUSION

326

327

328 329

330

331

332

333

334

Three Cenozoic subduction zones – Puysegur, IBM and Vanuatu – all show substantial components of strike–slip motion prior to and during initiation. Application of the mechanical model developed here using plate reconstruction constraints all yield estimates of initiation times consistent with values estimated independently from geological observations. Together, the models and observations suggest that subduction initiation can be triggered when margins become progressively weakened to the point that the resisting forces become smaller than the driving forces. Despite the strike-slip velocity having a relatively minor influence on the evolution of plate stress and initiation time compared to the plate convergent velocity, it can still dramatically lower the force required to induce subduction initiation, thereby providing a favorable condition for subduction initiation.

ACKNOWLEDGMENTS

- 335 Supported by the National Science Foundation through awards OCE-1654766, EAR-1645775, and OCE-
- 336 2049086. This work used Stampede-2 at the Texas Advanced Computer Center from the Extreme Science
- and Engineering Discovery Environment (XSEDE), which was supported by National Science Foundation.

SUPPLEMENTAL DATA

DATA AVAILABILITY STATEMENT

The datasets for this study can be found in the CaltechDATA at https://doi.org/110.22002/ae55y-m7q16.

REFERENCES

- 339 Arculus, R. J., Gurnis, M., Ishizuka, O., Reagan, M. K., Pearce, J. A., and Sutherland, R. (2019). How to
- 340 create new subduction zones: A global perspective. *Oceanography* 32, 160–174. doi:10.5670/oceanog.
- 341 2019.140
- 342 Auzende, J.-M., Lafoy, Y., and Marsset, B. (1988). Recent geodynamic evolution of the north Fiji basin
- 343 (southwest Pacific). *Geology* 16, 925–929
- 344 Beavan, J., Samsonov, S., Denys, P., Sutherland, R., Palmer, N., and Denham, M. (2010). Oblique slip
- on the Puysegur subduction interface in the 2009 July Mw 7.8 Dusky Sound earthquake from GPS and
- InSAR observations: implications for the tectonics of southwestern New Zealand. *Geophys. J. Int.* 183,
- 347 1265–1286. doi:10.1111/j.1365-246X.2010.04798.x
- 348 Bercovici, D. and Ricard, Y. (2014). Plate tectonics, damage and inheritance. Nature 508, 513-516.
- 349 doi:10.1038/nature13072
- 350 Bott, M. H. P. (1991). Ridge push and associated plate interior stress in normal and hotspot regions.
- 351 *Tectonophysics* 200, 17–32
- 352 Brune, J. N., Henyey, T. L., and Roy, R. F. (1969). Heat flow, stress, and rate of slip along the San Andreas
- Fault, California. J. Geophys. Res. 74, 3821–3827. doi:https://doi.org/10.1029/JB074i015p03821
- 354 Choi, H., Kim, S.-S., Dyment, J., Granot, R., Park, S.-H., and Hong, J. K. (2017). The kinematic evolution
- of the Macquarie Plate: A case study for the fragmentation of oceanic lithosphere. Earth and Planetary
- 356 *Science Letters* 478, 132–142
- 357 Collot, J. Y., Lamarche, G., Wood, R. A., Delteil, J., Sosson, M., Lebrun, J. F., et al. (1995).
- 358 Morphostructure of an incipient subduction zone along a transform plate boundary Puysegur Ridge and
- 359 Trench. Geology 23, 519–522. doi:Doi10.1130/0091-7613(1995)023(0519:Moaisz)2.3.Co;2
- 360 Crameri, F., Magni, V., Domeier, M., Shephard, G. E., Chotalia, K., Cooper, G., et al. (2020).
- A transdisciplinary and community-driven database to unravel subduction zone initiation. *Nature*
- 362 communications 11, 1–14
- 363 Faulkner, D. R., Mitchell, T. M., Jensen, E., and Cembrano, J. (2011). Scaling of fault damage zones with
- displacement and the implications for fault growth processes. Journal of Geophysical Research: Solid
- 365 *Earth* 116. doi:https://doi.org/10.1029/2010JB007788
- 366 Gurnis, M. (2023). An evolutionary perspective on subduction initiation. In *Dynamics of Plate Tectonics and*
- 367 *Mantle Convection*, ed. J. C. Duarte (Amsterdam: Elsevier). 357–383. doi:10.1016/B978-0-323-85733-8.
- 368 00003-2
- 369 Gurnis, M., Hall, C., and Lavier, L. (2004). Evolving force balance during incipient subduction.
- 370 Geochemistry Geophysics Geosystems 5. doi:ArtnQ0700110.1029/2003gc000681

- 371 Hall, C., Gurnis, M., Sdrolias, M., Lavier, L. L., and Müller, R. D. (2003). Catastrophic initiation of
- subduction following forced convergence across fracture zones. Earth Planet. Sci. Lett. 212, 15–30.
- 373 doi:10.1016/S0012-821X(03)00242-5
- Hall, R., Ali, J. R., Anderson, C. D., and Baker, S. J. (1995). Origin and motion history of the Philippine
- 375 Sea Plate. *Tectonophysics* 251, 229–250. doi:Doi10.1016/0040-1951(95)00038-0
- 376 Hightower, E., Gurnis, M., and Van Avendonk, H. (2020). A Bayesian 3-D linear gravity inversion for
- complex density distributions: application to the Puysegur subduction system. *Geophys. J. Int.* 223,
- 378 1899-1918
- 379 Hirth, G. and Kohlstedt, D. L. (1996). Water in the oceanic upper mantle: implications for rheology, melt
- extraction and the evolution of the lithosphere. Earth Planet. Sci. Lett. 144, 93–108
- 381 Hu, J. and Gurnis, M. (2020). Subduction duration and slab dip. Geochemistry, Geophysics, Geosystems
- 382 21. doi:10.1029/2019GC008862
- 383 Hu, J., Gurnis, M., Rudi, J., Stadler, G., and Müller, D. (2022). Dynamics of abrupt change in Pacific Plate
- motion around 50 Ma. *Nature Geoscience* 15, 74–78. doi:10.1038/s41561-021-00862-6
- 385 Humphreys, E. D. and Clayton, R. W. (1990). Tomographic image of the southern California mantle. J.
- 386 *Geophys. Res.* 95, 19725–19746
- 387 Ishizuka, O., Hickey-Vargas, R., Arculus, R. J., Yogodzinski, G., Savov, I. P., Kusano, A., Y. McCarthy,
- et al. (2018). Age of Izu Bonin Mariana arc basement. Earth Planet. Sci. Lett. 481, 80–90. doi:10.1016/
- 389 j.epsl.2017.10.023
- 390 Ismail-Zadeh, A. and Tackley, P. J. (2010). Computational Methods for Geodynamics (Cambridge, U.K.:
- 391 Cambridge University Press)
- 392 Kohlstedt, D. L., Evans, B., and Mackwell, S. J. (1995). Strength of the lithosphere: Constraints imposed
- by laboratory experiments. J. Geophys. Res. 100, 17,587–17602
- 394 Lallemand, S. and Arcay, D. (2021). Subduction initiation from the earliest stages to self-sustained
- subduction: Insights from the analysis of 70 Cenozoic sites. *Earth-Science Reviews* 221, 103779
- 396 Lamarche, G. and Lebrun, J.-F. (2000). Transition from strike-slip faulting to oblique subduction: active
- tectonics at the Puysegur margin, south New Zealand. *Tectonophysics* 316, 67—-89
- 398 Lebrun, J.-F., Lamarche, G., and Collot, J.-Y. (2003). Subduction initiation at a strike-slip plate boundary:
- 399 The Cenozoic Pacific-Australian plate boundary, south of New Zealand. Journal of Geophysical
- 400 Research: Solid Earth 108
- 401 Leng, W. and Gurnis, M. (2011). Dynamics of subduction initiation with different evolutionary pathways.
- 402 *Geochem. Geophys. Geosys.* 12. doi:10.1029/2011gc003877
- 403 Leng, W. and Gurnis, M. (2015). Subduction initiation at relic arcs. Geophysical Research Letters 42,
- 404 7014–7021. doi:10.1002/2015gl064985
- 405 Li, H.-Y., Li, X., Ryan, J. G., Zhang, C., and Xu, Y.-G. (2022). Boron isotopes in boninites document rapid
- changes in slab inputs during subduction initiation. *Nature communications* 13, 1–10
- 407 Li, Y. and Gurnis, M. (2022). A simple force balance model of subduction initiation. Geophysical Journal
- 408 *International* 232, 128–146
- 409 Mann, P. and Taira, A. (2004). Global tectonic significance of the solomon islands and ontong java plateau
- 410 convergent zone. *Tectonophysics* 389, 137–190
- 411 [Dataset] Mansour, J., Kaluza, O., Giordani, J., Beucher, R., Farringtona, R., Kennedy, G., et al. (2019).
- underworldcode/underworld2: v2.8.1b. doi:10.5281/zenodo.3384283
- 413 Maunder, B., Prytulak, J., Goes, S., and Reagan, M. (2020). Rapid subduction initiation and magmatism in
- the Western Pacific driven by internal vertical forces. *Nature Communications* 11, 1874

- 415 McKenzie, D. (1977). The initiation of trenches: a finite amplitude instability. In *Island arcs, deep sea*
- 416 trenches and back-arc basins, Maurice Ewing Series, eds. M. Talwani and W. Pitman (Washington, DC:
- 417 American Geophysical Union), vol. 1. 57–61
- 418 Moresi, L., Dufour, F., and Muhlhaus, H. B. (2003). A Lagrangian integration point finite element method
- for large deformation modeling of viscoelastic geomaterials. *Journal of Computational Physics* 184,
- 420 476–497. doi:PiiS0021-9991(02)00031-1Doi10.1016/S0021-9991(02)00031-1
- 421 Moresi, L., Gurnis, M., and Zhong, S. (2000). Plate tectonics and convection in the Earth's mantle: Toward
- a numerical simulation. *Comp. Sci. Engin.* 2, 22–33
- 423 Müller, R. D., Zahirovic, S., Williams, S. E., Cannon, J., Seton, M., Bower, D. J., et al. (2019). A
- 424 global plate model including lithospheric deformation along major rifts and orogens since the Triassic.
- 425 Tectonics 38, 1884–1907
- 426 Nikolaeva, K., Gerya, T., and Marques, F. (2010). Subduction initiation at passive margins: Numerical
- 427 modeling. J. Geophys. Res. 115. doi:10.1029/2009JB006549
- 428 Patriat, M., Falloon, T., Danyushevsky, L., Collot, J., Jean, M. M., Hoernle, K., et al. (2019). Subduction
- initiation terranes exposed at the front of a 2 Ma volcanically–active subduction zone. Earth Planet. Sci.
- 430 Lett. 508, 30–40. doi:10.1016/j.epsl.2018.12.011
- 431 Qing, J., Liao, J., Li, L., and Gao, R. (2021). Dynamic evolution of induced subduction through the
- inversion of spreading ridges. Journal of Geophysical Research: Solid Earth 126, e2020JB020965
- 433 Reagan, M. K., Heaton, D. E., Schmitz, M. S., Pearce, J. A., Shervais, J. W., and Koppers, A. P. (2019).
- Forearc ages reveal extensive short–lived and rapid seafloor spreading following subduction initiation.
- 435 Earth Planet. Sci. Lett. 506, 520—529. doi:10.1016/j.epsl.2018.11.020
- 436 Savage, H. M. and Brodsky, E. E. (2011). Collateral damage: Evolution with displacement of fracture
- distribution and secondary fault strands in fault damage zones. Journal of Geophysical Research: Solid
- 438 Earth 116. doi:https://doi.org/10.1029/2010JB007665
- 439 Shuck, B., Gulick, S. P. S., Van Avendonk, H. J. A., Gurnis, M., Sutherland, R., Stock, J., et al. (2022).
- Stress transition from horizontal to vertical forces during subduction initiation. *Nature Geoscience* 15,
- 441 149–155
- 442 Shuck, B., Van Avendonk, H., Gulick, S. P. S., Gurnis, M., Sutherland, R., Stock, J., et al. (2021).
- Strike-slip enables subduction initiation beneath a failed rift: New seismic constraints from Puysegur
- margin, New Zealand. *Tectonics* 40, e2020TC006436
- 445 Stern, R. J. and Bloomer, S. H. (1992). Subduction zone infancy examples from the Eocene Izu-
- Bonin-Mariana and Jurassic California arcs. Geol. Soc. Am. Bull. 104, 1621–1636. doi:Doi10.1130/
- 447 0016-7606(1992)104(1621:Szieft)2.3.Co;2
- 448 Sutherland, R., Barnes, P., and Uruski, C. (2006). Miocene-Recent deformation, surface elevation, and
- volcanic intrusion of the overriding plate during subduction initiation, offshore southern Fiordland,
- 450 Puysegur margin, southwest New Zealand. N.Z. J. Geol. Geophys. 49, 131–149
- 451 Sutherland, R., Dickens, G. R., Blum, P., Agnini, C., Alegret, L., Asatryan, G., et al. (2020). Continental-
- scale geographic change across Zealandia during Paleogene subduction initiation. *Geology* 48. doi:10.
- 453 1130/G47008.1
- 454 Thielmann, M. and Kaus, B. J. P. (2012). Shear heating induced lithospheric-scale localization: Does it
- result in subduction? *Earth Planet. Sci. Lett.* 359, 1–13. doi:10.1016/j.epsl.2012.10.002
- 456 Torsvik, T. H., Doubrovine, P. V., Steinberger, B., Gaina, C., Spakman, W., and M., D. (2017). Pacific
- plate motion change caused the Hawaiian-Emperor bend. *Nature Communications* 8
- 458 Toth, J. and Gurnis, M. (1998). Dynamics of subduction initiation at preexisting fault zones. *Journal of*
- 459 Geophysical Research-Solid Earth 103, 18053–18067. doi:Doi10.1029/98jb01076

- 460 Whittaker, J. M., Muller, R. D., Leitchenkov, G., Stagg, H., Sdrolias, M., Gaina, C., et al. (2007).
- Major Australian–Antarctic plate reorganization at Hawaiian–Emperor bend time. *Science* 318, 83–86.
- 462 doi:10.1126/science.1143769
- 463 Yang, G. (2022). Subduction initiation triggered by collision: A review based on examples and models.
- 464 Earth-Science Reviews, 104129
- 465 Zhong, X. and Li, Z.-H. (2019). Forced subduction initiation at passive continental margins: Velocity-driven
- versus stress-driven. Geophys. Res. Lett. 46, 11054–11064
- 467 Zhong, X. and Li, Z.-H. (2023). Compression at strike-slip fault is a favorable condition for subduction
- initiation. Geophysical Research Letters 50, e2022GL102171
- 469 Zhou, X., Li, Z.-H., Gerya, T. V., J., S. R., Xu, Z., and Zhang, J. (2018). Subduction initiation dynamics
- along a transform fault control trench curvature and ophiolite ages. *Geology* 46, 607–610. doi:10.1130/
- 471 G40154.1
- 472 Zoback, M. D., Zoback, M. L., Mount, V. S., Suppe, J., Eaton, J. P., Healy, J. H., et al. (1987). New
- evidence on the state of stress of the San Andreas Fault system. Science 238, 1105–1111. doi:10.1126/
- 474 science.238.4830.1105

FIGURE CAPTIONS

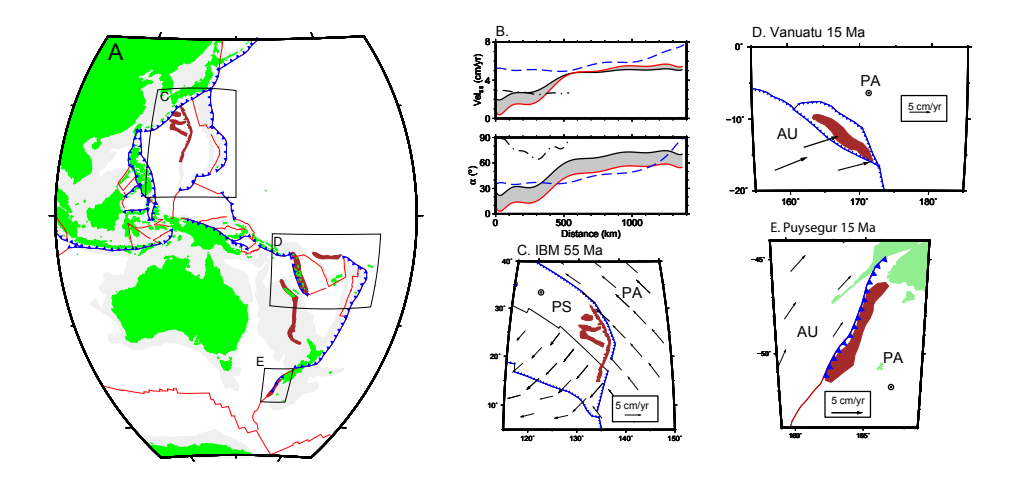


Figure 1. Three Cenozoic subduction initiation events that occurred in the western Pacific showing a substantial component of relative, strike-slip motions at the nascent trench just prior to initiation. A. Present-day western Pacific with the structures against which subduction initiated shown in brown. Regions of detail shown with boxes. B. Magnitude of strike slip motion (above) and convergence direction (below, with 0 being normal to the strike of the trench) before onset of initiation. Izu-Bonin-Mariana (IBM) shown at 55 Ma (red) and 50 Ma (black solid) with values for intermediate times shown with with grey shading, Vanuatu at 15 Ma (blue dashed) and Puysegur (black, dot-dashed) using the plate model of Müller et al. (2019). C. Conditions at IBM at 55 Ma, 5 Myr before the onset of SI. D. Vanuatu at 15 Ma, 1-3 Myr before onset. E. Puysegur at 15 Ma, 1-3 Myr before onset. Abbreviations for plates: PA-Pacific Plate, AU-Australia Plate, PS-Philippine Sea Plate

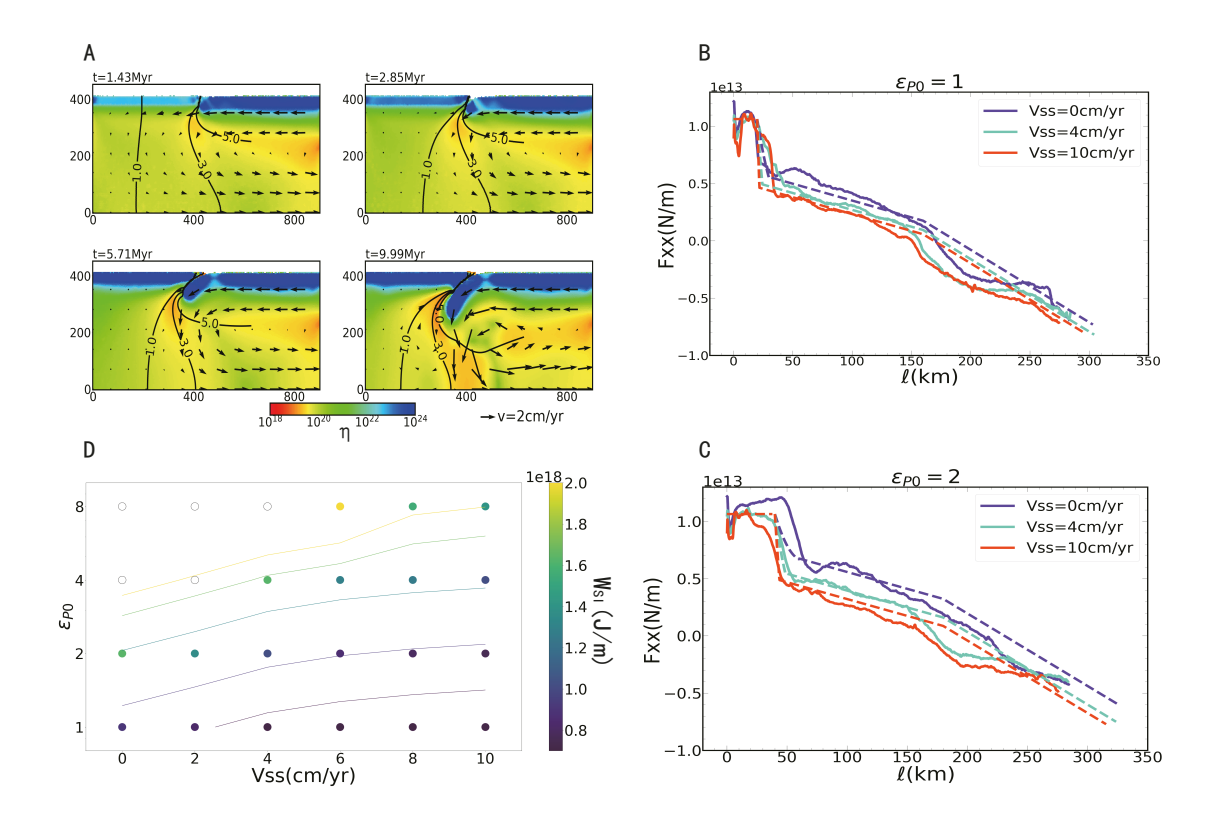


Figure 2. (A) An example of model with 1cm/yr convergent velocity. Color shows the effective viscosity. Vectors show the in-plane component velocity and contours show strike slip velocity in cm/yr. (B) The integrated horizontal compressional force in the plate F_{xx} as a function of plate motion ℓ for models with different strike slip velocity V_{SS} under $\varepsilon_{P0}=1$. Solid line for numerical model results and dashed line for analytical results. (C) Same as (B) but with slower weakening rate $\varepsilon_{P0}=2$. (D) The work done to initiate a subduction W_{SI} of every numerical model(color-coded solid circle) in the parametric grid search varying the strike slip velocity V_{SS} and ε_{P0} . Contours show the prediction of W_{SI} from analytical model.

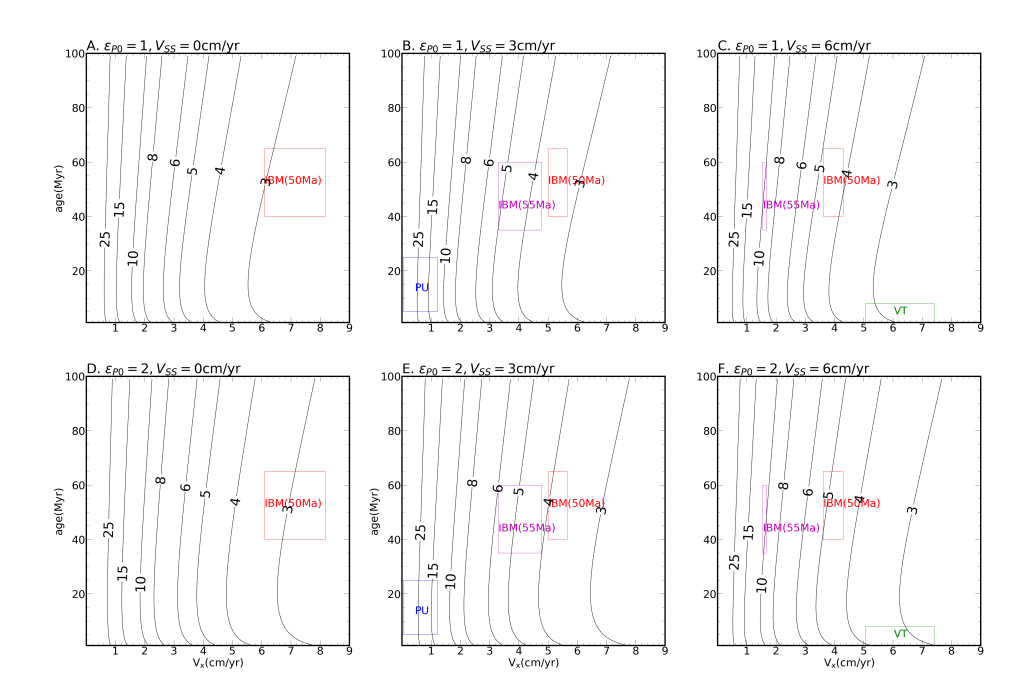


Figure 3. Analytical prediction of initiation time t_{SI} under different convergent velocity Vx and subducting plate age with A. $V_{SS}=0$, $\varepsilon_{P0}=1$, B. $V_{SS}=3\mathrm{cm/yr}$, C. $V_{SS}=6\mathrm{cm/yr}$, $\varepsilon_{P0}=1$. D to F are the same as A to C except $\varepsilon_{P0}=2$. Red, magenta, blue and green box show the parameter range of IBM (50Ma), IBM (55Ma), Puysegur (PU) and Vanuatu (VT) subduction initiation from the given V_{SS} with a $\pm 1\mathrm{cm/yr}$ range.

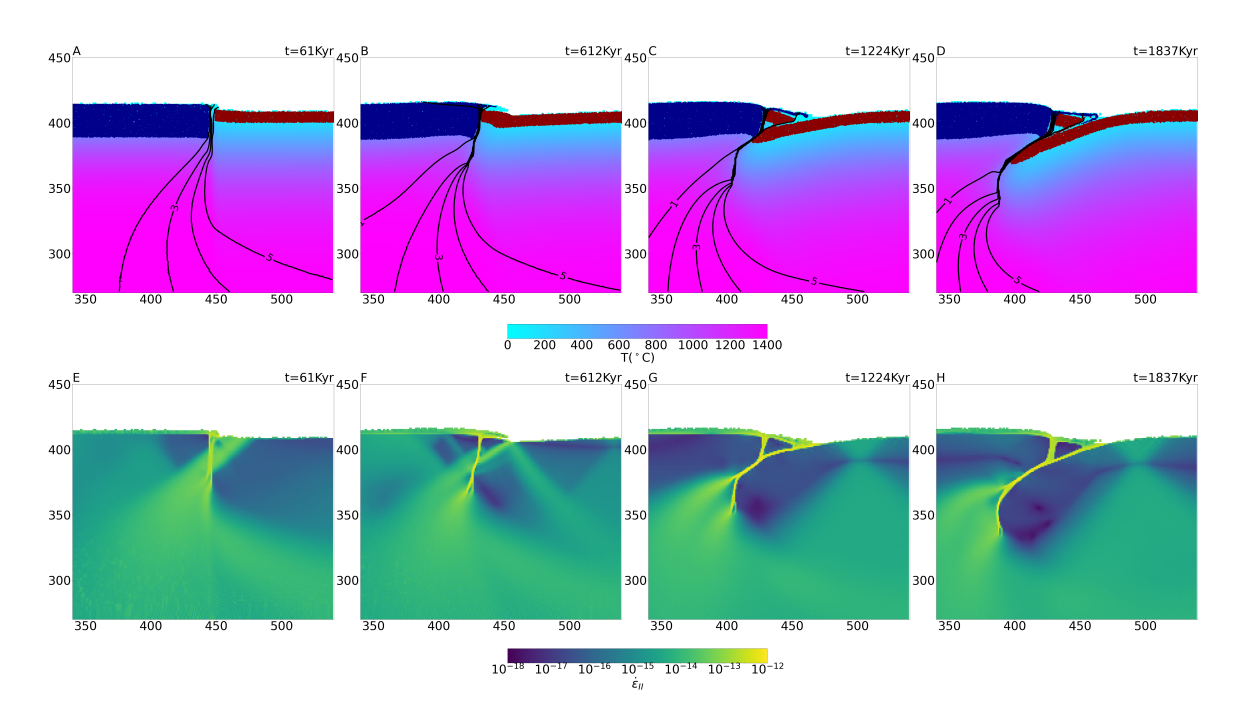


Figure 4. Fault evolution of a high resolution models with $[\varepsilon_{P0}, V_{SS}, V_p]$ =[2, 6 cm/yr, 4 cm/yr]. A–D Red and blue for oceanic and continental crust. Background color for temperature. E–H Second invariant of strain rate $(\dot{\varepsilon}_{II})$.